Structural modifications of carbon–carbon composites under high temperature and ion irradiation

T. Paulmier[a], M. Balat-Pichelin[a,*], D. Le Quéau[b]

[a]Laboratoire Procédés, Matériaux et Energie Solaire, PROMES-CNRS (ex IMP-CNRS),
UPR 8521, BP 5, Font-Romeu Odeillo 66125, France
[b]Centre d'Etude Spatiale des Rayonnements, CESR-CNRS, UPR 2592,
9 av. du Colonel Roche, Toulouse, Cedex 431028, France

Abstract

Carbon–carbon composites are the most interesting materials for the conception of the thermal shield of the solar probe space mission designed to study the solar wind and solar corona. The physico-chemical behavior and the structural modifications of some carbon–carbon composites at high temperature and under proton irradiation have been studied using SEM, XRD and Raman spectroscopy. The characterization of the as-received carbon–carbon composites show that the processing routes and the fiber preform have a strong influence on the microstructure of the composites: the fibrous preform 2.5D, the liquid consolidation and a final heat treatment allows to enhance drastically the graphitization degree of the carbon matrix and the fibers and the size of the crystallites. The high temperatures induce especially a decrease of the open porosity due to an amorphous carbon deposit at the surface of the material. This evolution has been observed mainly for the 2.5D structure. The high temperatures come to an evolution of the microstructure with a better crystallinity, an increase of the size and orientation of the crystallites of the fibers and matrix. The 2D structure presents, however, an increase of the disorder with the temperature.

Finally, the hydrogen irradiation has only a very weak influence on the inner and surface degradation of the carbon–carbon composites.

1. Introduction

Several space missions (Solar Probe [1,2], Solar Orbiter [3]) are currently in progress to explore the sun environment and carry out in situ measurements on the

* Corresponding author. Tel.: +33 468307768;
fax: +33 468302940.
E-mail address: balat@promes.cnrs.fr (M. Balat-Pichelin).

solar wind and the solar corona. These spacecrafts will be submitted at their perihelion to severe aggressions coming from the sun. It is thus necessary to protect them from the intense solar flux using a thermal shield, which will allow to the shipped-in instruments to work without damages and disturbances.

Carbon–carbon composites are the most interesting materials for the conception of the thermal shield due to their high melting point, low density, good strength-to-weight ratio and good thermo-radiative properties with high values and a stable ratio of solar absorptivity to total hemispherical emissivity [4,5]. It is also very easy to modify their physical and thermal properties by acting on the processing routes and the morphology of the fibers and weave.

The solar probe, whose perihelion will be at four solar radii from the sun, will be submitted to an hydrogen ion flux of 5×10^{16} ions m^{-2} s^{-1} with an energy of 2 keV. The surface of the carbon thermal shield will be heated at temperatures between 1800 and 2400 K. These different aggressions will induce a structural degradation of the material, a mass loss and the emission of a secondary atmosphere, which may pollute the spacecraft and disturb the in situ measurements.

It is thus necessary for the conception of a reliable and non-disturbing thermal shield to study the physico-chemical behavior and the structural modifications of the carbon–carbon composites at high temperature and under proton irradiation.

In a previous paper [6], the physico-chemical sputtering processes of the carbon–carbon composites at temperatures up to 2400 K and irradiated by H$^+$ ions have been studied and evaluated. The erosion processes of carbon materials irradiated by hydrogen ions at high temperature have been identified by theoretical and experimental studies. The mass loss rate, the composition and the nature of the neutral and ionized species emitted by the carbon–carbon composites and the influence of the processing routes on the sputtering processes have been measured.

This paper deals with the structural evolution of the carbon–carbon composites under the same experimental conditions. A first study also allowed to determine the influence of the processing routes on the structure and morphology of the carbon–carbon composites.

Only a few experiments exist on the evolution of carbon–carbon composites under high vacuum, submitted to temperature above 1800 K and irradiated by H$^+$ ions. This work allows to understand the influence of the temperature, the ion irradiation and the processing routes on the structural behavior of these composites.

2. The experimental set-up

A test facility called MEDIASE (Moyen d'Essai et de Diagnostic en Ambiance Spatiale Extrême) has been developed and instrumented to simulate the solar environment (Fig. 1). This test facility is placed at the focus of the 1000 kW solar furnace in Odeillo, France. The materials are heated under high vacuum up to 2500 K using the solar concentrated radiation, which allows to reach high temperatures in a few seconds. The set-up is composed of a chamber, with a capacity of around 0.06 m^3, equipped with a turbomolecular pump (Leybold 450, 0.45 m^3 s^{-1} pumping speed) together with a roots pump, which permits to reach a pressure of about 10^{-7} h Pa. A hemispherical silica-glass window, 35 cm in diameter, is placed in front of this chamber and allows to irradiate the front face of the samples with the solar beam of the 1000 kW solar furnace. This sample, 40 mm in diameter and 2–3 mm thick, are maintained in a water-cooled holder with three metallic or ceramic needles to minimize the heat flow from the sample to the holder. The front face of the chamber, which receives the concentrated solar flux, is also water-cooled.

On the back face of the sample, temperature, mass loss, optical and mass spectrometry measurements are possible due to a water-cooled measuring chamber keeping free the instruments from parasitic radiation of the surroundings. Finally, several tubes have been placed around the chamber to insert the ion source and the measuring instruments. The samples are irradiated on their back face by H$^+$ ions with an ion source (Fisons, EX05). The ions flux is 5×10^{16} ions m^{-2} s^{-1} with an energy of 2 keV. The ion irradiation of the sample is maintained during the whole period of the sample heating. The temperature of the material is measured using an original optical-fiber bi-chromatic pyrometer, especially designed in our laboratory for in situ measurements under severe conditions.

MEDIASE

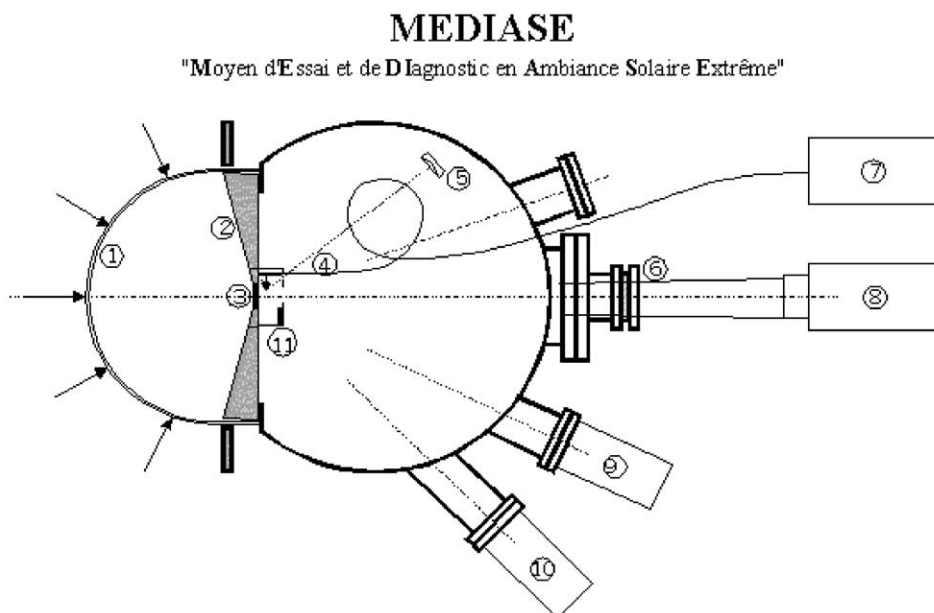"Moyen d'Essai et de Diagnostic en Ambiance Solaire Extrême"

Fig. 1. MEDIASE experimental set-up: (1) hemispherical quartz window, (2) water-cooled holder, (3) sample, (4) optical fiber, (5) quartz microbalance, (6) viewport, (7) bi-chromatic optical pyrometer, (8) mass spectrometer, (9) and (10) two positions (30° and 45°) for the UV source and ion source.

Several in situ measurements have been carried out first on the carbon–carbon composites: mass loss rate, mass spectrometry and temperature. These measurements have allowed to identify the different physico-chemical sputtering processes [6]. Post-treatment analyses are then performed on the material to evaluate their structural damages due to the high temperatures and the ion irradiation. To understand the influence of the above parameters on the degradation of the material, two steps of experimental tests have been carried out: the samples were (i) only heated, (ii) heated and irradiated by H^+ ions. Accordingly, three kind of samples have been analysed: as-received, treated at high temperature and treated at high temperature under ion irradiation. The treated samples have been successively heated and irradiated or not during 30 min at 1800 K, 30 min at 2100 K, 5 min at 2400 K.

The post-treatment analyses allowed to study the evolution of three main parameters: the surface morphology, evaluated by scanning electronic micro-scopy (SEM), the surface defect concentration evaluated by Raman spectroscopy (incident beam: 647.1 nm, size of the spot: 3 μm) and the crystallinity

and structural orientation by X-ray diffraction (XRD; X-ray incident beam at 0.15406 nm).

These above analytic tools have also been used to study the influence of the processing routes and weave on the structure of the carbon–carbon composites. The density, the porosity and the specific surface area of the different as-received carbon materials have been measured. The densities have been evaluated with a helium pycnometer (AccuPyc 1330). The specific surface area measurements have been realized with a BET equipment (ASAP2010 Micromeretics using Kr). Finally, the porosities of the materials have been measured with a mercury porosimeter (Micromeretics Autopore III WIN 9420).

The carbon materials, which have been tested are four industrial carbon–carbon composites (called A, B, F and G), which differ from their weave, their fibrous preform and their processing route (Table 1). The fibers of the four composites are (PAN) polyacrilonitrile-based carbon fibers. Composite A presents a 2D weave structure, contrary to the other three composites, which structure is 2.5D. The 2D weave correspond to the superimposition of flat fiber clothes, forming a fiber lap. The 2.5D structure

Table 1
Technical characteristics of the different carbon–carbon composite materials studied

Samples	A	B	F	G
Fiber		Ex-PAN HR		Ex-PAN HR
Fibrous preform	2D	2.5D	2.5D	2.5D
Weave		Twill weave		Plain weave
Liquid consolidation	Yes	Yes	No	No
Matrix fabrication method	CVI (1300 K)	CVI (1300 K)	CVI (1300 K)	CVI (1300 K)
Final thermal treatment (K)	2470	2470	No	2470

Table 2
Physical characteristics of the different carbon–carbon composite materials studied

Samples	Density (g cm^{-3})	Specific surface area (m^2 g^{-1})	Porosity (%)	Pore size (μm) and distribution (%)
F	1.82 ± 0.01	0.15 ± 0.006	6	0.1–4 (59) 4–30 (20) 30–300 (21)
G	1.81 ± 0.01	0.35 ± 0.006	17	0.05–30 (83) 30–300 (17)
A	1.73 ± 0.02	0.17 ± 0.006	12	0.1–30 (80) 30–300 (20)
B	1.75 ± 0.03	0.40 ± 0.006	14	30–300 (100)

corresponds to the needle-punching of this fiber lap in order to tie up the fibers together, forming a 3D weave structure. The composites A and B have been submitted to a first liquid consolidation before the matrix fabrication. This consolidation, carried out with a liquid resin, allows tying up the carbon fibers and strengthens the weave. The matrix of the four composites has been produced by chemical vapor infiltration (CVI) at 1300 K. The CVI process used here is a gas phase infiltration using a volatile hydrocarbon for the fabrication of the matrix. The fiber weave is heated and the gas is then thermally decomposed, resulting in a deposit of pyrolytic carbon. Contrary to composite F, composites A, B and G have then been annealed at 2470 K in an inert atmosphere and under atmospheric pressure.

3. Characteristics of the as-received carbon–carbon composites

In a first step, the as-received carbon–carbon composites have been characterized to understand the importance of the processing routes and the fibrous preform on their structure.

Table 2 presents the density and the porosity of the different carbon–carbon composites.

3.1. The diffraction spectra of the carbon–carbon composites

Fig. 2 presents the XRD spectrum of the carbon–carbon composite B. The same feature is observed for the four current composites. The spectra of the carbon–carbon composites present two peaks corresponding to the reflection peaks 0 0 2 and 0 0 4 at around 26° and 54°. Another asymmetric peak is observed for a diffraction angle equal to 42°. The interpretation of this peak is very tricky and would imply a deconvolution. However, because of the low intensity of the peak, this deconvolution would be very difficult and the experimental uncertainty very wide.

From the large width of the reflection peak 0 0 2 and its position corresponding to an inter-plane graphite distance higher than 3.39 Å, we can deduce that the graphitization degree of the carbon–carbon composites is very low. The observed shoulder and the large width of this peak are actually due to the presence of two 0 0 2 reflection peaks corresponding to the fibers (the lowest diffraction angle correspond-
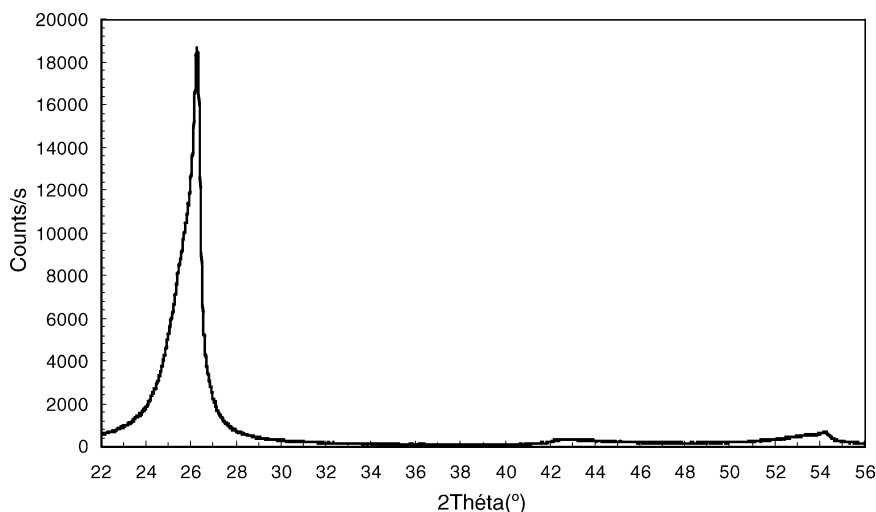
Fig. 2. Overall XRD spectra of the as-received C/C composite B.

ing to the least crystallized phase) and the matrix, respectively. For the carbon–carbon composites A and B, it is possible to carry out a deconvolution of the 0 0 2 reflection peak and identify the two different peaks (Table 3). The distribution of the fibers and the fibrous preform strongly acts on the fiber–matrix interface causing stress, cracks and voids in the matrix [7]. The presence of the carbon fibers thus induces many defects, pores and a large amount of disoriented graphenes, coming to a low graphitization degree.

3.2. The Raman spectra of the carbon–carbon composites

The Raman spectra reveal three peaks for each carbon–carbon composites (Fig. 3):

- The first one located at 1580 cm^{-1} (I_G) corresponds to the graphite network.
- Two other peaks located at 1330 (I_D) and 1620 cm^{-1} corresponds, respectively to the finite size of the crystallites and to the defects in the carbon fibers and the matrix [8].

Due to the width of the beam in Raman spectroscopy, the analysis comprises the matrix of the composite, their fiber and the matrix around the fibers. The intensity of the peaks is not revealing, since it depends on the position of the beam on the sample. It is however possible to determine the size of the crystallites from the ratio I_D/I_G using the Knight and White formula [8] (Table 4). The ratio I_{1620}/I_G allows to evaluate the defect concentration in the composites. As we can see on Fig. 3 and Table 4, the size of the crystallites and the defect concentration strongly depend on the fibrous preform and the processing routes. The effect of the different operating parameters (liquid consolidation, heat treatment) and the fiber architecture on the Raman spectra are discussed in Sections 3.4–3.6.

3.3. The surface morphology of the carbon–carbon composites

The surface morphology of the carbon–carbon composites has been analysed by SEM with three magnifications (2000, 6000 and 10,000). The magnifications 6000 reveal a carbon coating at the surface of the carbon composites (Fig. 4). We will see in Section 3.5 that the morphology of this pyrocarbon coating [9,10] strongly varies with the substrate and the fiber architecture.

The carbon coating observed on the fibers has been deposited during the production of the matrix by chemical vapor infiltration. In CVI process, pyrolitic

Table 3
$c/2$ parameters (Å) measured for the composites A and B

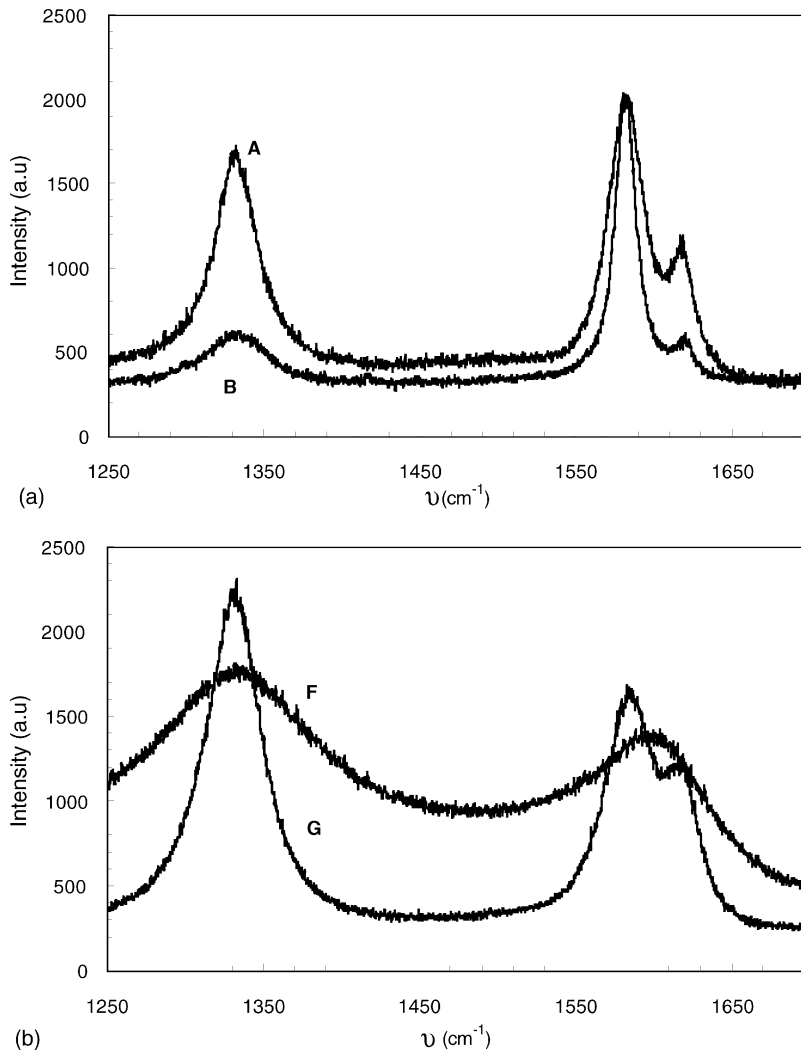| Samples	First peak (carbon fiber)	Second peak (carbon matrix)
A	3.49	3.42
B	3.46	3.39

Fig. 3. Raman spectra of the as-received C/C composites: (a) composites A and B, (b) composites F and G.

carbon tend to deposit at the surface of the composite being fabricated, blocking the surface porosity [11]. This pyrocarbon is produced by nucleation and growth on the surface of the fibers, as described in [9]. The surface of the non-crystalline carbon fibers presents a high concentration of active sites, which controls the pyrocarbon deposit and the morphology of this carbon coating [11].

3.4. Influence of the final heat treatment during the processing route

Comparing Tables 1 and 2, we can see that the heat treatment performed during the processing route of the composites does not act on the density but especially on the porosity of the material. The inner porosity of the composite F (6%), which has

Table 4
Crystallites size and disorder degree evaluated by Raman spectroscopy on the as-received carbon–carbon composites

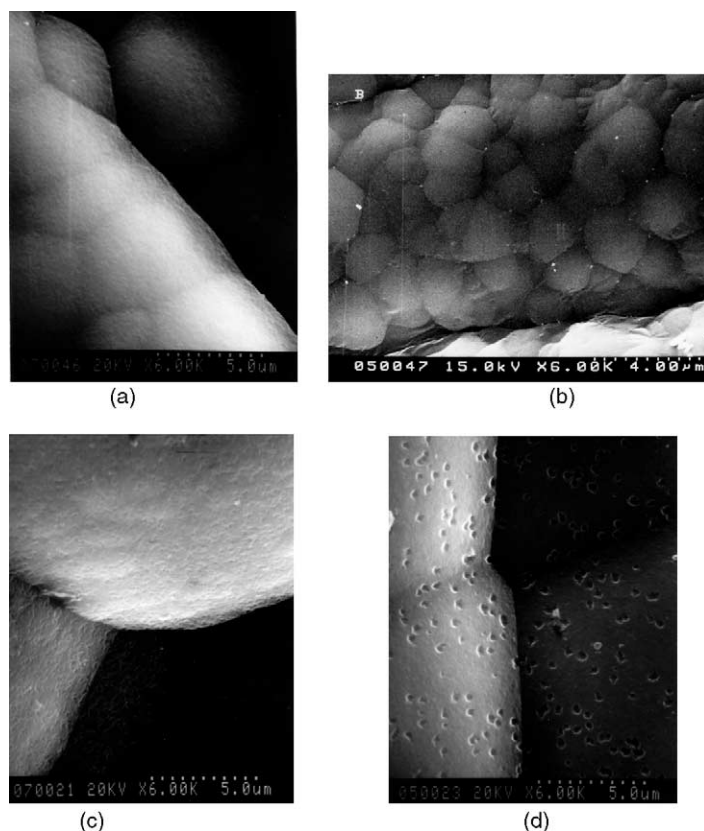| Samples	I_D/I_G	I_{1620}/I_G	Size of crystallites L_a (Å)
F	1.30	–	34
G	1.18	0.60	37
A	0.85	0.57	52
B	0.31	0.29	143

Fig. 4. SEM micrograph (magnification: 6000) of the as-received composites: (a) composite A, (b) composite B, (c) composite F and (d) composite G.

not been submitted to a final heat treatment during its elaboration process, is then three times lower than the composite G (17%), which presents the same fiber, weave and texture. We can see by SEM micrographs that the open porosity of the composite G is much larger than for the composite F (Fig. 4). The effect of the heat treatment (2470 K) is thus to enhance the migration of the pores towards the material surface: this effect decreases the inner porosity and increases the open porosity. This migration induces the emission of hydrocarbons (outgassing) initially present in the porous structure. This effect has already been demonstrated [6,12].

The effect of the heat treatment during the elaboration process can be observed on the diffraction spectra of the composites F and G. Fig. 5 shows that the peak 0 0 2 of the heat-treated composite G is more intense and corresponds to an inter-plane graphite distance lower than for the composite F. The heat treatment furthers the graphitization and enhances the crystallite size.

The Raman spectra are in agreement with the results obtained by XRD. We can see in Table 4 that the crystallite size is slightly higher for composite G than for F. For composite F, the two peaks I_D and I_{1620} merge due to its high disorder degree (Fig. 3). The heat treatment allows therefore to improve the structural organization of the carbon–carbon composites. We can notice in Table 2 that the heat treatment increases the porosity and the specific area of the carbon–carbon composites. The process has been described by Ko et al. [12]: in the non-heat-treated composite, the number of functional groups is very important coming to strong fiber–matrix bonding. The heat treatment enhances the carbonization of the fibers and the matrix; the fiber–matrix bonding is then lower, which increases the close porosity of the carbon–carbon composite. Moreover, the thermal expansion coeffi-
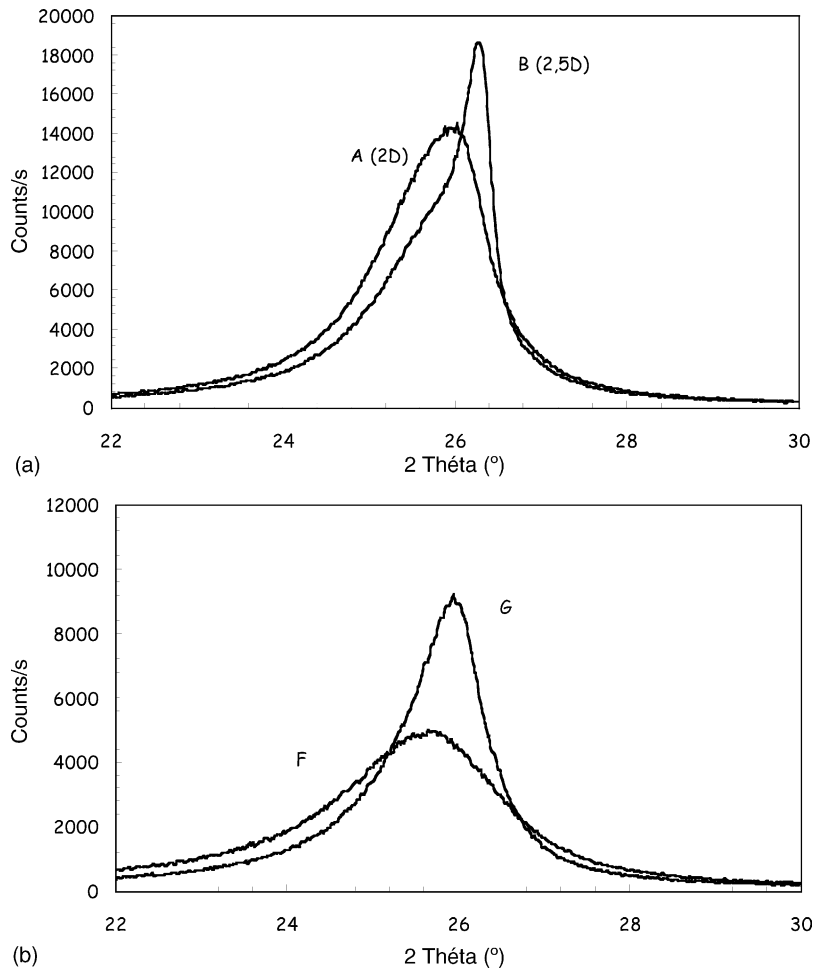
Fig. 5. XRD spectra of the as-received C/C composites (0 0 2 peak): (a) composites A and B, (b) composites F and G.

cients of the fiber and the matrix are different and a number of cracks can be observed between the fiber and the matrix.

3.5. Influence of the fibrous preform

The fibrous preform has also a strong influence on the structure and the surface morphology of the carbon–carbon composites. During the matrix processing, the deposition processes are in fact strongly dependent of the fibrous shape and preform [10]. Composites A and B only differ by the fibrous preform: they present a 2D and 2.5D structures, respectively. The XRD spectra (Fig. 5) of the

composite B shows a sharper and higher intense peak than for the composite A: the crystallite size, along the *c*-axis, is larger for the 2.5D structure. The Raman analysis (Table 4) confirms this result since the crystallites size, along the *c*-axis, of the composite B is three times larger than for the composite A. The 2.5D preform structure furthers therefore, the crystallite growth. The SEM micrographs (Fig. 4) show that the fibrous preform strongly acts on the deposition process: we can actually notice that the morphology of the carbon coating deposited on the fibers drastically varies from composite A to composite B, which differ only by the fiber architecture. The main reason is that the fiber weave strongly act on the

surface area (Table 2): it has been demonstrated [10] that the main parameter controlling the chemisorption and deposition of the pyrocarbon coating is the surface area. The fibrous preform acts also on the distribution of the pores without changing the pore concentration: the size of the pores for the composite B, which presents a 2.5D preform, is higher than 30 μm whereas the pores of the composite A is mainly lower than 30 μm (Table 2).

Ma et al. [11] have shown that, in the case of a 2D structure, cracks and pores are observed in the matrix between the fiber laps. The 2.5D structure ties up the fiber laps with carbon fibers allowing increasing the

fiber laps bonding, getting a higher graphitization degree of the matrix and avoiding shrinkage of this carbon matrix.

3.6. Influence of the liquid consolidation

The liquid consolidation is realized before the processing of the carbon matrix to strengthen the weave and protect the carbon fibers. Composites A and B have been submitted to a liquid consolidation. For these composites, it is possible to calculate the parameter $c/2$ for the two phases (Table 3). The comparison between the XRD spectra of composites A–B and composites
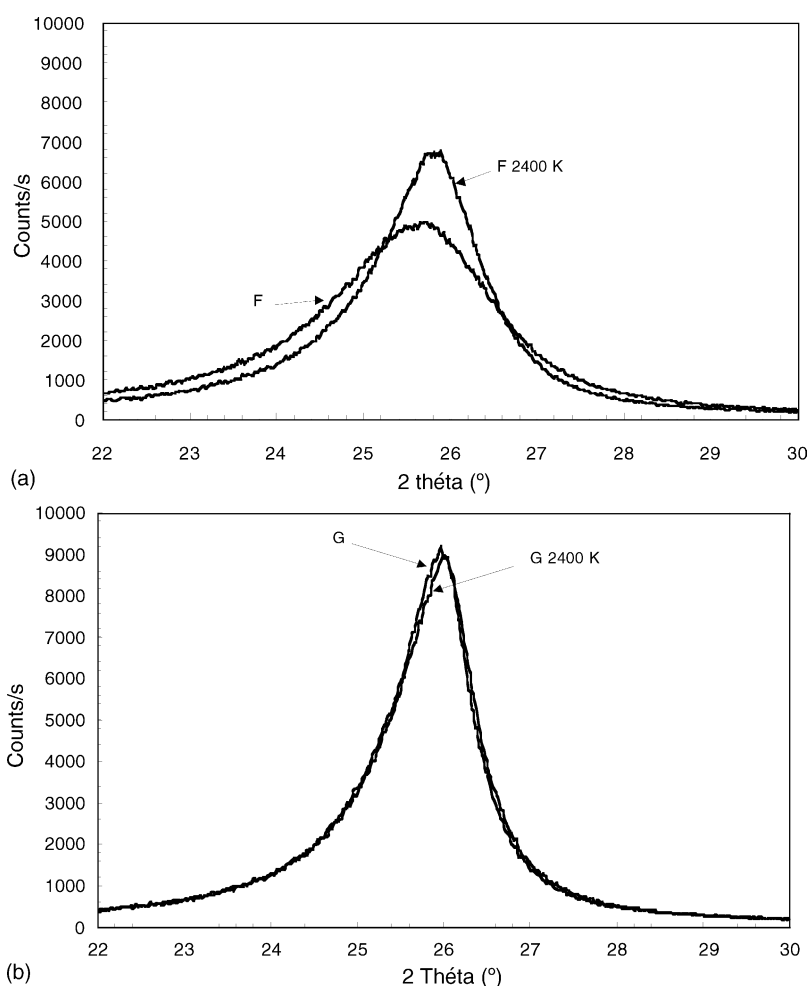

Fig. 6. XRD spectra (0 0 2 peak) of the as-received and heat-treated (2400 K without ion irradiation) C/C composites: (a) composite F, (b) composite G, (c) composite A and (d) composite B.
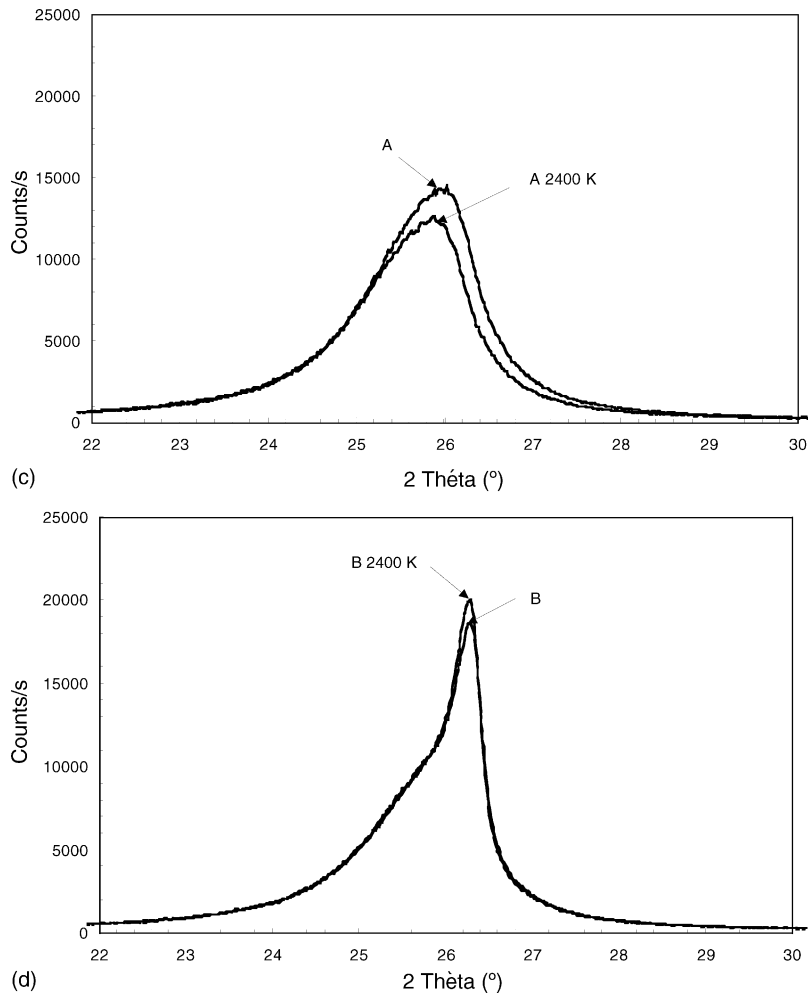
(c)

(d)

Fig. 6. (*Continued*).

F–G (Fig. 5) reveals that the graphitization degree along the *c*-axis is much higher for the composites submitted to a liquid consolidation. The density of composites A and B, submitted to a liquid consolidation, present however a slightly lower density than composites F and G, which could be explained by a slightly higher material withdrawal during the heat treatment.

The Raman spectroscopic measurements show that the crystallites of composites A and B are larger than for composites F and G (Table 4) and confirm the higher degree of crystallinity due to the liquid consolidation. The defect concentration (evaluated by the ratio I_{1620}/I_G) is also slightly lower for composite A and hugely lower for composite B.

We can see on the SEM micrographs that the composite G, which has been submitted to a similar processing route and weave as the composite B except the liquid consolidation, presents an important open porosity, which is not observed for the composite B (Fig. 4).

3.7. Synthesis

From this first set of characterization of the as-received carbon–carbon composites, it appears that the

processing routes and the fiber preform have a strong influence on the microstructure of the composites. To summarize, the fibrous preform 2.5D, the liquid consolidation and a final heat treatment allow to enhance drastically the graphitization degree of the carbon matrix and the fibers, the size of the crystallites along the *c*-axis and the defect concentration.

4. Evolution of the structure of carbon–carbon composites at high temperature

According to the bibliographic study [13–15], the high temperature and the ion irradiation induce an evolution of the surface morphology and the microstructure of the carbon materials. A first study has allowed us to study the physico-chemical behavior of the carbon–carbon composites by measuring their mass loss rate, the composition and the distribution of the neutral and ionized emitted gas [6]. It is however important to analyse in a second step the surface and the inner degradation of the composites by a post-treatment analysis using three techniques (SEM, XRD and Raman spectroscopy). The surface morphology and the lattice structure are strongly related to the thermo-radiative properties of the carbon material and thus to a possible variation of its temperature.

In a first step, the carbon–carbon composites have been treated at high temperature up to 2400 K according to the experimental protocol described in Section 2. The evolution of the structure under high vacuum has been studied for each kind of carbon–carbon composites. The degradation process and the amplitude strongly depend on the processing routes and the fiber preform. As described in Section 3, these two parameters have an influence on the surface morphology and the microstructure (defects concentration, crystallites size, crystallinity) of the as-received carbon–carbon composites. The structural changes will be lower since the carbon–carbon composites will be well graphitized.

4.1. Evolution of the inner structure of the carbon–carbon composites

The analysis of the samples by XRD after the heat treatment performed in the MEDIASE set-up shows that the degree of crystallization of the composites increases. Fig. 6 presents the peak 0 0 2 of as-received and treated samples up to 2400 K for the four C/C composites.

The peak 0 0 2 of the composite F moves towards the larger angles (corresponding to a lower *c* parameter). The intensity of the peak increases and its width decreases, which means that crystallites are much better oriented and that the size of these crystallites increases (along to the *c*-axis). All the carbon–carbon composites tested in this study have this same characteristics, but it is more emphasized for the composite F in so far as this composite has not been annealed during its processing. We can notice that the structure of the 2400 K heated composite F is closed to the structure of the composite G. The inner structure of composite B is not altered contrary to composite A (Fig. 6), which is submitted to a distortion of the mean crystalline network, characterized by a decrease of the intensity of the peak (0 0 2). An increase of the parameter d_{002} is also observed for composite A treated at 2400 K, corresponding to a decrease of the crystallinity of this composite. This observation has also been confirmed by Raman spectroscopy where we can notice an increase of the intensity of the D peak, corresponding to the increase of defects and decrease of crystallite size. The 2D composites are therefore less tolerant to the high temperature treatment than 2.5D composites. This can be due to the increase of close porosity or the formation of cracks, induced by thermal stresses, between the fiber laps for the 2D composite [11].

4.2. Evolution of the surface structure of the carbon–carbon composites

Fig. 7 shows the Raman spectra of the as-received and heat-treated samples for the four C/C composites. The most revealing changes can be observed again for composite F: the width of the different peaks drastically decreases corresponding to an increase of the crystallinity. The spectrum of the heated composite F is then close to composite G. No changes can be observed for the 2.5D structures (composites B and G). The high temperatures have no influence on the defect concentration of the composites since the relative intensity of I_{1620} comparing to I_G does not change with the high

temperature. We can however observe an increase of the intensity of peak I_D for composite A corresponding to a decrease of the crystallite size, in agreement with the XRD measurements presented in Section 4.1. The 2D fibrous preform is therefore submitted to damages and stresses of its inner structure at high temperature.

4.3. Evolution of the morphology of the carbon–carbon composites

The evolution of the morphology of the carbon–carbon composites has been analysed by SEM. The most revealing changes have been observed for magnification higher than 10,000. At this scale,

we study the surface morphology of the carbon fibers.

Three main features can be distinguished according to the nature of carbon–carbon composites (Figs. 8–10):

- No significant changes observed for composites A and F (Fig. 8 for composite F).
- A decrease of the open porosity is observed for composite G (Fig. 9). The size of the pores is divided by 2.
- For composite B, the cone structure of the pyrocarbon coating has disappeared: the surface is then smooth (Fig. 10).
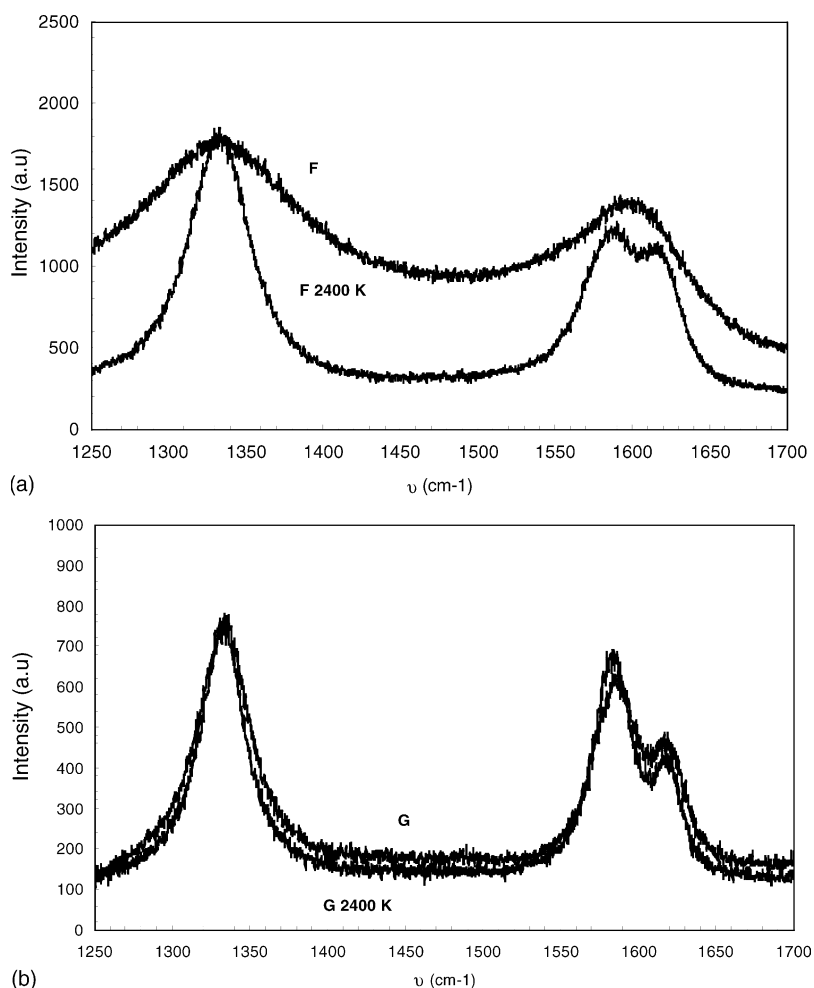

Fig. 7. Raman spectra of the as-received and heat-treated (2400 K without ion irradiation) C/C composites: (a) composite F, (b) composite G, (c) composite A and (d) composite B.
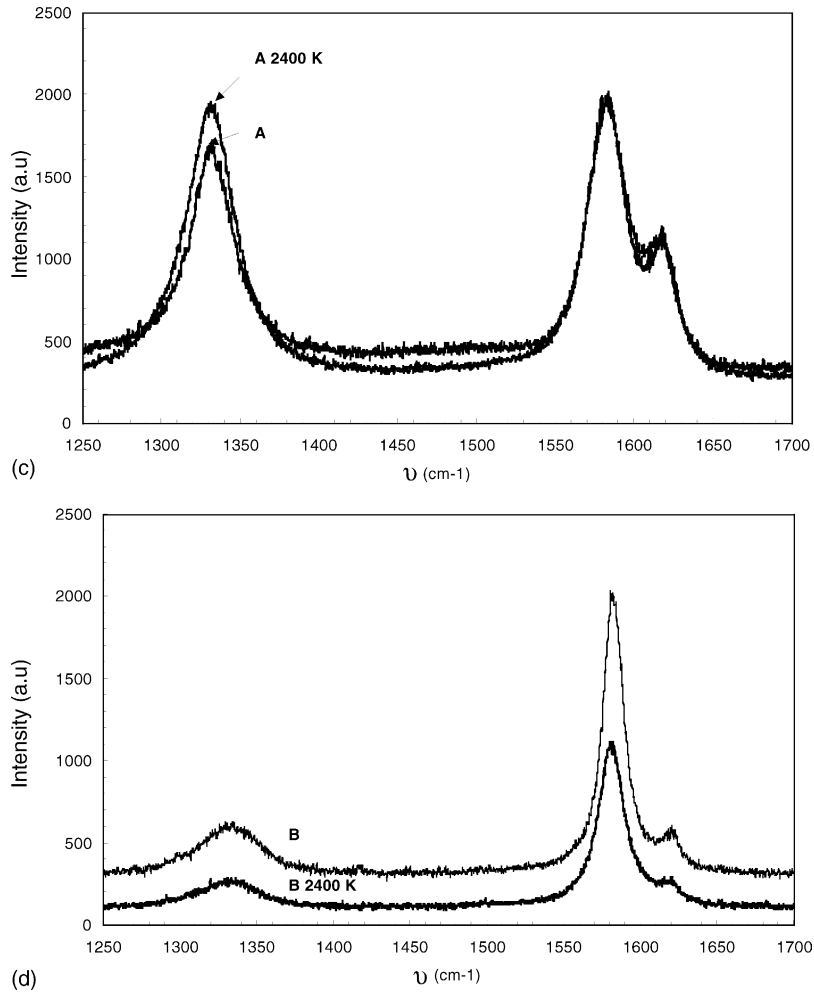
(c)

(d)

Fig. 7. (*Continued*).

The evolution of composites B and G can be explained by an amorphous carbon deposit at the surface of the material, on the coldest zone of the surface, inside of the open pores. This has already been demonstrated by Ko et al. in the case of pores on carbon fibers during the CVI process [16]. This deposit can be observed visually especially on the front face of the sample, which is submitted to a higher temperature: an amorphous deposit characterized by a brown color has been identified. This kind of carbon deposit at the surface of graphite samples has already been observed and explained by

Wachi and Gilmartin [17]. During the heat treatment, the carbon composites are vaporized and emit a large amount of carbon species. The vaporization and the deposit processes strongly depend on the morphology and the orientation of the crystallites: this can thus explain the differences observed between the carbon–carbon composites. A part of the vaporized carbon species is deposited at the surface of the material. The deposit processes especially depend on the concentration of cold zones due to the thermal gradient induced by the rugosity and open porosity of the material: the composites B and G,
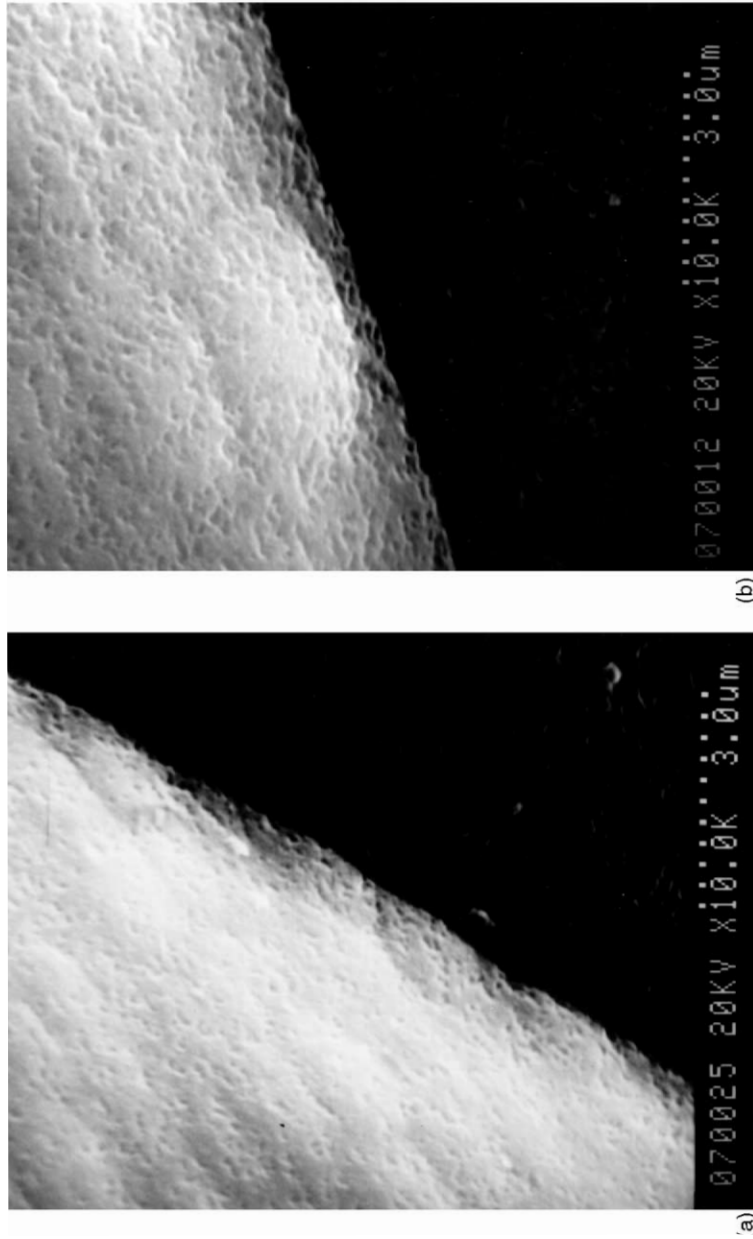
Fig. 8. SEM micrograph (magnification: 10,000) of composite F: (a) as-received, (b) heat-treated (2400 K without ion irradiation).
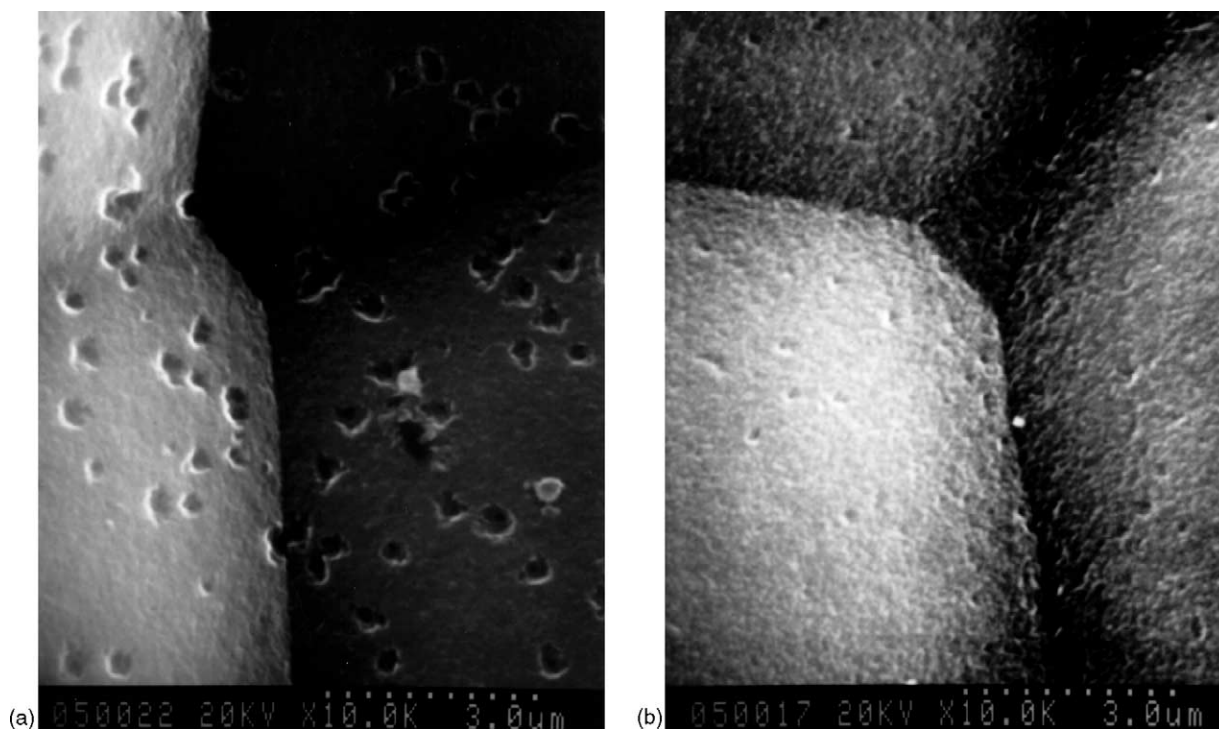
Fig. 9. SEM micrograph (magnification: 10,000) of composite G: (a) as-received, (b) heat-treated (2400 K without ion irradiation).

which present the most porous and cone structures, are thus submitted to an important carbon deposit, as we can see on Figs. 9 and 10. The amorphous carbon is emitted from the composite during the outgassing stage. This has already been demonstrated in a previous study [6]: a high amount of hydrocarbon is released during this stage. The emission of the gases induces the formation of pores at the surface of the fibers, which are the main location of the further deposit [16]. A part of these emitted hydrocarbons can also be decomposed during the high treatment (especially at higher temperature than the processing one), resulting in the deposition of this amorphous carbon.

5. Evolution of the structure of carbon–carbon composites at high temperature and ion irradiation

In a second step, the carbon–carbon composites have been treated at high temperature and irradiated by H^+ ions. The XRD, Raman and SEM measurements have revealed that the ion irradiation induces no significant changes on the inner structure and the morphology of the carbon–carbon composites. In the literature, the carbon–carbon composites have been irradiated by H^+ ions at relatively low temperature comparing to the current experimental temperature range. These studies concern especially the thermal protection for the fusion reactor Tokamak. They have shown a degradation on the surface of the carbon–carbon composites [18]. This difference is due to the fact that the temperature is much lower (around 1000 K) in the tests for Tokamak shield than in our experimental tests. The temperature thus seems to have an annealing effect on the possible degradations induced by ion irradiation. The defects produced in the carbon lattice by hydrogen impact are then annealed at high temperature. The high temperature especially furthers the diffusion and the emission of the implanted ion hydrogen, which may induce cracks and pores at lower temperature.
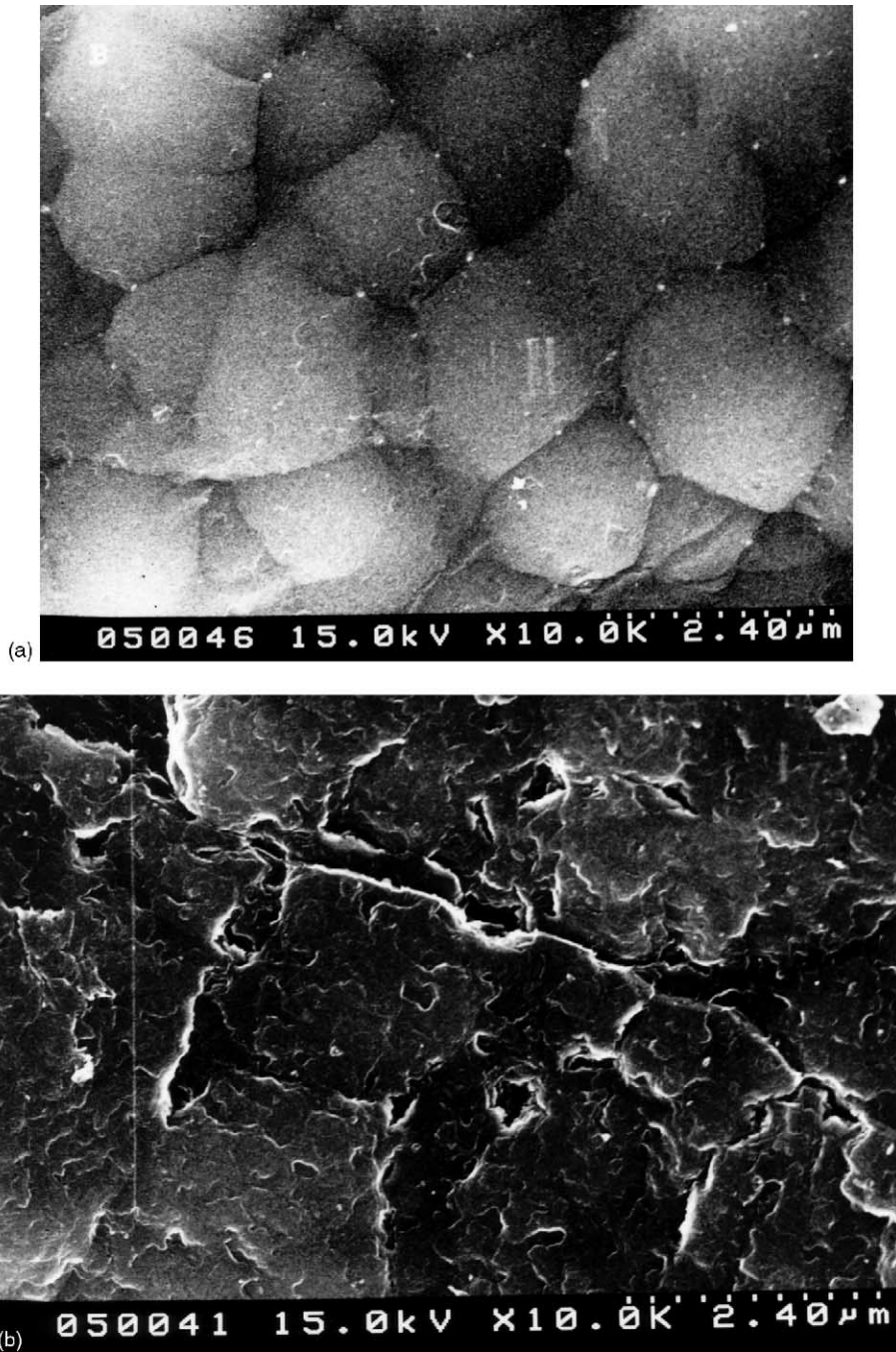
(a)

050046 15.0kV X10.0K 2.40μm

(b)

050041 15.0kV X10.0K 2.40μm

Fig. 10. SEM micrograph (magnification: 10,000) of composite B: (a) as-received, (b) heat-treated (2400 K without ion irradiation).

6. Conclusion

This study has been divided into two main points: (i) the influence of the processing routes and fiber weave on the morphology and the structure of the carbon–carbon composites, (ii) the evolution of the structure and morphology of the carbon–carbon composites at high temperature and ion irradiation under a high vacuum.

The processing routes and the fiber architecture have a strong influence on the crystallinity, the porosity and the morphology of the carbon–carbon composites. The fibrous preform (2D or 2.5D) acts especially on the crystallinity of the matrix and the size of its crystallites. The 2.5D architecture then increases these two parameters. The heat treatment furthers the crystallinity of the matrix and fibers but tends to increase the close and open porosity of the material. The liquid consolidation also enhances the crystallinity of the matrix and fibers, decreases the defect concentration and allows to have a low open porosity.

The structural degradation of the carbon–carbon composites strongly depends on the processing routes and the fibrous preform. These two parameters have a strong influence on the surface area and the microstructure, which acts on the surface temperature of the material, and on its mass loss rate.

The high temperatures induce especially a decrease of the open porosity due to an amorphous carbon deposit at the surface of the material. A high amount of hydrocarbons are released during the outgassing of the composites at high temperature and then thermally fragmented and deposited at the surface of the material. This evolution has been observed mainly for the 2.5D structure. The high temperatures come to an evolution of the microstructure with a better crystallinity, an increase of the size and the orientation of the crystallites of the fibers and matrix. The 2D structure presents however an increase of the disorder with the temperature and a decrease of the crystallinity of the composite. This decrease must be due to the thermal stresses between the fiber laps at high temperature, which has been already observed in the literature.

Finally, the hydrogen irradiation between 1800 and 2400 K has only a very weak influence on the inner and surface degradation of the carbon–carbon composites: this is due to the too low energy (2 keV) and ion flux (5×10^{16} ions m^{-2} s^{-1}). The main reason is that the high temperatures anneal the possible degradations due to the ion irradiation, observed at low temperature. STM observation of the carbon fibers would certainly allow to study the influence of the ion irradiation at an atomic scale.

As a consequence from this study, one of the most interesting PAN-based carbon–carbon composites for the conception of the solar probe thermal shield are those which have been submitted to a post-heat treatment, a liquid consolidation and with a 2.5D structure. This must be confirmed by studying the thermo-radiative properties of these carbon–carbon composites, which are predominant for the evaluation of the temperature of the material.

References

[1] J. Randolph, J. Ayon, R. Dirling, W. Imbriale, R. Miyake, D. Le Quéau, G. Olalde, E. Pierson, S. Rawal, B. Rivoire, J.F. Robert, C. Royère, R. Taylor, P. Valentine, W. Vaughn, The solar probe shield/antenna materials characterization, Carbon 37 (1999) 1731–1739.

[2] G. Gloeckler, S.T. Suess, S.R. Habbal, R.L. Mcnutt, J.E. Randolph, A.M. Title, B.T. Tsurutani, J.L. Burch, R.L. Carovillano, S.K. Antiochos, Solar probe: a mission to the sun and the inner core of the heliosphere. Sun-Earth plasma connections, Geophys. Monogr. 109 (1999) 237–246.

[3] G. Colangelo, O. Pace, R. Marsden, B. Fleck, Solar orbiter: a challenging mission design for near-sun observations, ESA Bull. 104 (2000) 76–85.

[4] J.M. Millard, R.N. Miyake, R.B. Dirling, A. Rolfo, C. Royere, Starprobe thermal shield evolution, in: Proceedings of the International Symposium on Environmental and Thermal Systems for Space Vehicles, Toulouse, France, 1983, pp. 531–560.

[5] O. Vaisberg, N. Tsurutani, in: Proceedings of the First US-Russian Scientific Workshop on FIRE Environment, Space Research Institute, Moscow, Russia, 1995.

[6] T. Paulmier, M. Balat-Pichelin, D. Le Quéau, R. Berjoan, J.F. Robert, Physico-chemical behavior of carbon materials under

high temperature and ion irradiation, Appl. Surf. Sci. 180 (2001) 227–245.

[7] S.P. Appleyard, B. Rand, The effect of fiber–matrix interactions on structure and property changes during the fabrication of unidirectional carbon–carbon composites, Carbon 40 (2002) 817–834.

[8] M.S. Dresselhaus, R. Kalish, Raman spectroscopy, in: Ion Implantation in Diamond, Graphite and Related Materials, Springer Verlag, 1992 pp. 59–63.

[9] N. Murdie, C.P. Ju, J. Don, M.A. Wright, Carbon–carbon matrix materials, in: J.D. Buckley, D.D. Edie (Eds.), Carbon–carbon Materials and Composites, William Andrew Publishing, Noyes, 1993, Chapter 5, pp. 105–167.

[10] P. Delhaes, Chemical vapor deposition and infiltration processes of carbon materials, Carbon 40 (2002) 641–657.

[11] C.-C.M. Ma, N.-H. Tai, W.-C. Chang, Y.-P. Tsai, Morphologies, microstructure and mechanical properties of 2D carbon–carbon composites during the CVI densification process, Carbon 34 (1996) 1175–1179.

[12] T.-H. Ko, W.-S. Kuo, Y.-H. Chang, Influence of carbon fibers felts on the development of carbon–carbon composites, Composites: Part A 34 (2003) 393–401.

[13] M.S. Dresselhaus, R. Kalish, Ion implantation, in: Ion Implantation in Diamond, Graphite and Related Materials, Springer Verlag, 1992 pp. 26–37.

[14] M. Balooch, D.R. Olander, Reactions of modulated molecular beam with pyrolitic graphite, III, Hydrogen, J. Chem. Phys. 63 (11) (1975) 4772–4786.

[15] J. Roth, J. Bohdansky, W. Poschenrieder, M.K. Sinha, Physical and chemical sputtering of graphite and SiC by hydrogen and helium in the energy range of 600–7500 eV, J. Nucl. Mater. 63 (1976) 222–229.

[16] T.-H. Ko, W.-S. Kuo, S.-S. Tzeng, Y.-H. Chang, The microstructural changes of carbon fiber pores in carbon–carbon composites during pyrolysis, Compos. Sci. Technol. 63 (2003) 1965–1969.

[17] F.M. Wachi, D.E. Gilmartin, High temperature mass spectroscopy, free vaporisation studies of graphites, Carbon 8 (1970) 141–154.

[18] G. Federici, C.H. Skinner, J.N. Brooks, J.P. Coad, C. Grisolia, A.A. Haasz, A. Hassanein, V. Philipps, C.S. Pitcher, J. Roth, W.R. Wampler, D.G. Whyte, Plasma-material interactions in current Tokamaks and their implications for next step fusion reactors, Nucl. Fusion 41 (2001) 1967–2137.